Journal of
Marine Science and Engineering

MDPI

Article

Effect of High-Stress Levels on the Shear Behavior of Geosynthetic-Reinforced Marine Coral Sands

Lixing Liu [1,2,3], Zhixiong Chen [3,4,*], Xuanming Ding [3,4] and Qiang Ou [3,4]

[1] State Key Laboratory of Precision Blasting, Jianghan University, Wuhan 430056, China; llx1063089550@163.com
[2] Hubei Key Laboratory of Blasting Engineering, Jianghan University, Wuhan 430056, China
[3] College of Civil Engineering, Chongqing University, Chongqing 400045, China; dxmhhu@163.com (X.D.); ouq126@cqu.edu.cn (Q.O.)
[4] Institute for Smart City of Chongqing University in Liyang, Changzhou 213300, China
* Correspondence: chenzhixiong@cqu.edu.cn

Abstract: As an important construction material, the mechanical and deformation properties of marine coral sand determine the safety and stability of related island and coastal engineering construction. The porous and easily broken characteristics of coral sand often make it difficult to meet engineering construction needs. In particular, coral sand undergoes a large amount of particle breakage under high-stress conditions, which in turn negatively affects its mechanical and deformation properties. In this study, the macro- and micro-mechanical behavior of geosynthetic-reinforced coral sand under high confining pressure was investigated and compared with unreinforced cases using the three-dimensional discrete element method (DEM), which was verified by indoor triaxial tests. The results showed that the stress–strain responses of unreinforced and reinforced coral sand under high confining pressure showed completely different trends, i.e., the hardening tendency shown in the reinforced case. Geosynthetic reinforcement can significantly inhibit the stress–strain softening and bulging deformation of coral sand under high confining pressure, thus improving the shear mechanical performance of the reinforced sample. At the microscopic scale, high confining pressure and reinforcement affected the contact force distribution pattern and stress level between particles, determining the macroscopic mechanical and deformation performance. In addition, the breakage of particles under high confining pressure was mainly affected by shear strain and reinforcement. The particle fragment distribution, particle gradation, and relative breakage index exhibited different trends at different confining pressure levels. These breakage characteristics were closely related to the deformation and stress levels of unreinforced and reinforced samples.

Keywords: marine coral sand; triaxial test; DEM simulation; high confining pressure; shear mechanical behavior; particle breakage

Citation: Liu, L.; Chen, Z.; Ding, X.; Ou, Q. Effect of High-Stress Levels on the Shear Behavior of Geosynthetic-Reinforced Marine Coral Sands. *J. Mar. Sci. Eng.* **2024**, *12*, 2081. https://doi.org/10.3390/jmse12112081

Received: 17 October 2024
Revised: 8 November 2024
Accepted: 9 November 2024
Published: 18 November 2024

1. Introduction

With the development and utilization of the oceans, a large number of islands and coastal infrastructures have been built on sites with coral sand as the core filler [1,2], especially in tropical and subtropical regions. Coral sand is a special calcareous sand formed by the remains of marine organisms over a long period of evolution. The main component of coral sand is calcium carbonate, which usually contains a large number of pores [3]. Due to the abundance of marine organism remains, the physical properties of coral sands formed, such as shape, angularity, porosity, hardness, etc., show some variability, making its mechanical properties more complex than those of standard quartz sands [1,4]. Coral sands are also subject to granular breakage under high stress, leading to alterations in the gradation characteristics [4–6] and the corresponding mechanical properties. Attention to the mechanical properties of coral sands in the construction of islands and marine projects is essential for the safety of the superstructures and adjacent infrastructures.

In recent years, the mechanical and bearing behavior of coral sands received widespread attention as a series of engineering projects advanced in areas where coral sands are widely distributed [7–9]. A series of experimental [4,6,10,11], numerical [12–14], and theoretical studies [10,15,16] have focused on the basic mechanical properties of coral sands in an attempt to reveal their special characteristics. Since multi-angularity and particle breakage are typical characteristics of coral sands [6,10,17], exploring angular properties and particle breakage is an important aspect of understanding the mechanical and bearing behavior of coral sands. Several recent studies showed that the angular and breakage properties of coral sand play opposite roles in the mechanical behavior [12,13,18]. This is manifested by the fact that angular properties favor the enhancement of inter-particle occlusion, which in turn contributes positively to shear strength. However, particle breakage, in turn, disrupts the inter-granular occlusion, resulting in stress release, which in turn leads to a reduction in the shear strength. This opposite action complicates the mechanical behavior of coral sand and is not conducive to the needs of current engineering and construction.

To reduce the influence of undesirable properties, such as low hardness, porosity, and particle breakage, on the shear mechanical behavior of coral sands, a series of reinforcement methods to enhance the stability of coral sands are the focus of current research, such as cement-curing technology [19,20], bio-curing technology [21,22], and geosynthetic reinforcement technology [23–26]. Among them, geosynthetic reinforcement technology, which is less polluting to the marine environment and has significant advantages, such as low cost and high efficiency, is a potential method for the future reinforcement of large coral sand sites and geotechnical structures [27–29]. Ding et al. [30] investigated the shear behaviors of unreinforced and geosynthetic-reinforced coral sands based on an indoor triaxial test, and the results showed that reinforcement can significantly improve the mechanical and deformation properties of coral sands. In addition, a series of experimental and numerical studies related to coral sand reinforced with geosynthetics were carried out to compare important aspects, such as shear strength [23,25], deformation [30–32], liquefaction resistance [24,27], and bearing capacity, before and after reinforcement [31]. These studies provided valuable insights for the construction of island and coastal projects. Nevertheless, most of the performed triaxial tests have focused on confining pressures below 400 kPa [30,33,34], and little attention is given to the shear mechanical behavior of unreinforced and reinforced coral sands under high confining pressures. The degree of breakage of coral sand will be increased under high confining pressure, and its interaction with geosynthetics and the effect of reinforcement may undergo new changes. Therefore, conducting investigations under high confining pressure levels is necessary to enhance the current understanding of the shear mechanical behavior of unreinforced and reinforced coral sands.

Considering that recent studies on reinforced coral sands have mainly focused on confining stresses up to 400 kPa, the mechanical behavior at higher stresses is still unclear. To investigate the macro/micro-shear mechanical behavior of unreinforced and reinforced coral sands at higher stress levels, triaxial shear investigations in the range of 400 kPa~1600 kPa confining pressure are carried out in this study using the validated DEM method. Mechanical and deformation analyses at the macro and micro levels are performed to reveal the shearing mechanisms of high confining pressure levels and geosynthetic reinforcement on coral sands. The stress–strain response, shear strength, shear mechanical parameters, failure patterns, microscopic contact force characteristics, and particle fragmentation distributions of unreinforced and reinforced coral sands are also evaluated in detail. Further, the potential connection between the macroscopic mechanical response and the microscopic stresses and particle fragmentation is also revealed under high confining pressures.

2. Materials and Methods

2.1. Geologic Background and Lithologic Characteristics of Marine Coral Sands

Tropical and subtropical seas between 30 degrees south and 30 degrees north latitude of the Earth harbor a large number of coral-like organisms. These marine organisms

reproduce rapidly, and over tens of thousands of years of evolution, their remains are deposited on the seafloor, gradually accumulating to form calcareous cement. Its main components are the less stable aragonite and calcite, and the content of quartz is usually less than 10%. The composition of this mineral results in low mechanical strength and particle hardness. In recent years, with the construction of oceanic island projects, the calcareous aggregates deposited on the seafloor have been hydraulically blown onto the islands and reefs as important foundation materials. Typically, the fill material for island reef sites is coral sand with smaller particles.

Coral sand is formed through the long-term evolution of the remains of marine organisms. Its calcium carbonate content is usually above 80% and even exceeds 90%. Thus, the main mineral components of coral sand particles are aragonite and calcite. Due to the long-term effects of the marine environment, the coral sand particles have many pores and corners, and their shape is irregular. Figure 1 shows the coral sand used in the indoor triaxial test [30], with a gradation of 0–2 mm. Tests showed that the specific gravity of coral sand was 2.78, and the porosity ratio ranged from 0.79 to 1.24. As shown in Figure 1b, the abundant corners made the interlocking of the coral sand particles prominent, which further complicated its mechanical properties [35,36]. In addition, due to the low hardness of coral sand, the irregular particle shape and internal pores further increased the possibility of stress concentration [37]. Therefore, coral sand particles often undergo significant particle breakage under high-stress levels. After basic particle shape testing, the sphericity of the planar image of coral sand particles was significantly lower than that of standard sand, mainly ranging from 0.2 to 0.8. Among them, the strip (branch) particles had the lowest sphericity, mainly below 0.5. Particle breakage was not only related to stress, but also closely related to shear strain and particle properties. Currently, the particle breakage of coral sand is a point of concern.

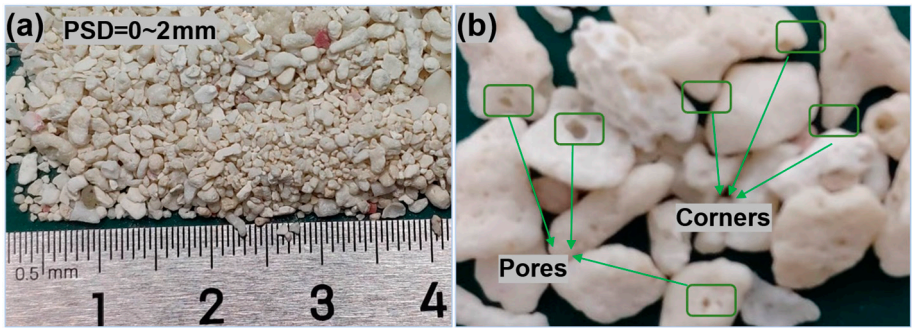

Figure 1. Shape characteristics of coral sand particles: (**a**) coral sand from the South China Sea, and (**b**) angularity and porosity characteristics.

To further explore the effect of high confining levels on the shear mechanical behavior of unreinforced and reinforced coral sand, the DEM method was used to simulate the behavior of coral sand particles. Considering that abundant corners and fragmentation are basic properties of coral sand particles, the sand particles were constructed based on the method of breakable cemented particles, and the specific technical details are consistent with the research carried out by Luo et al. [12] and Peng et al. [18]. According to the proportion characteristics of real coral sand in Figure 1, a 4:1 relationship was employed to determine the sizes of the host particles and angular particles. The specific particle geometric characteristics and contact model are shown in Figure 2. The angular particles were symmetrically distributed at the four vertices of a regular tetrahedron and were bonded to the host particles by a parallel bond model [38]. Once the stress between the particles exceeded the allowable bond strength, the bond between the host particles and the angular particles broke, and the angular particles fell off. The broken particles were filled into the pores as small particles using a linear model. Such DEM simulations can reflect the breakage of coral sand particles and the impact on the grading curve. In the

DEM simulation, the particle size distribution (PSD) was modified according to the actual grading of the triaxial test [30] in the laboratory and enlarged to the range of 1–3 mm. Research conducted by Wang et al. [39] indicated that the use of grading modification and size enlargement techniques can achieve the simulation of the basic mechanical properties of soil while ensuring computational efficiency.

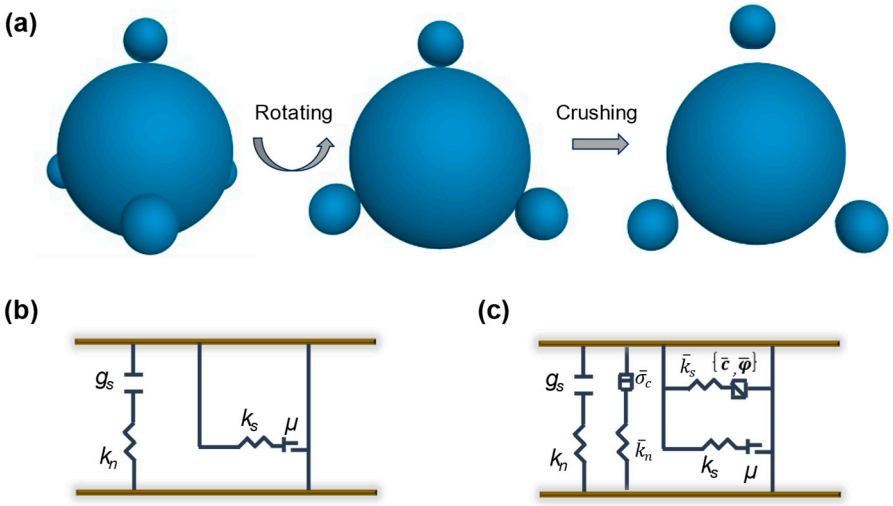

Figure 2. 3D coral sand particle construction and microscopic contact models based on DEM: (**a**) 3D DEM particle, (**b**) linear contact model, and (**c**) linear parallel bonding model.

2.2. Overview of Triaxial Tests and DEM Simulations

A DEM model verified by the triaxial test was used to conduct the numerical simulation. In the indoor triaxial test [30], the diameter and height of the specimen were 80 mm and 39.1 mm, respectively. To reflect the physical laws in the test, a triaxial DEM specimen of the same size was constructed, with a total number of particles exceeding 100,000. In order to ensure the efficiency of calculation, the particle size in DEM was 1 mm~3 mm, which was obtained by adjusting and enlarging according to the grading characteristics in the test. The relative densities of the experimental and numerical soil samples were kept essentially the same to avoid the effect of densification differences on shear behavior. The characteristics of the specimen in the test and the numerical test are shown in Figure 3. In this case, the three layers of the geogrid remained evenly distributed in the reinforced specimen. The geogrid was constructed from a series of 2 mm-diameter spherical particles and was given its tensile strength by a parallel bonding model. In the DEM simulation, the compaction conditions of the specimen were consistent with the laboratory triaxial test, and the test procedures were carried out in sequence, including equilibrium, consolidation, and loading. The maximum axial strain during loading was 20%. After loading, the stress–strain relationship was obtained using a monitoring program. For deviatoric stress–strain curves without significant peaks, the stress corresponding to 15% strain was regarded as the shear strength. In the linear contact model, the normal/shear stiffness of the geogrid and coral sand was 2×10^8 N/m. In the parallel bonding model, the normal/shear stiffness of the geogrid and coral sand was 2×10^8 N/m^3 and 5×10^8 N/m^3, respectively, and their bonding strengths were 1×10^9 Pa and 9×10^9 Pa, respectively. To ensure the validity of the numerical simulation, the triaxial test and DEM simulation were verified in terms of stress–strain, particle breakage, and failure patterns of the specimen. The results of the validation showed that the method was effective for simulating the shear mechanical behavior of unreinforced and reinforced coral sand. The specific determination of microscopic contact parameters and model validation refers to the research carried out by Luo et al. [12]. The validated numerical model can be used to further carry out macro/microscopic shear mechanical analysis of unreinforced and reinforced coral sand at high-stress levels.

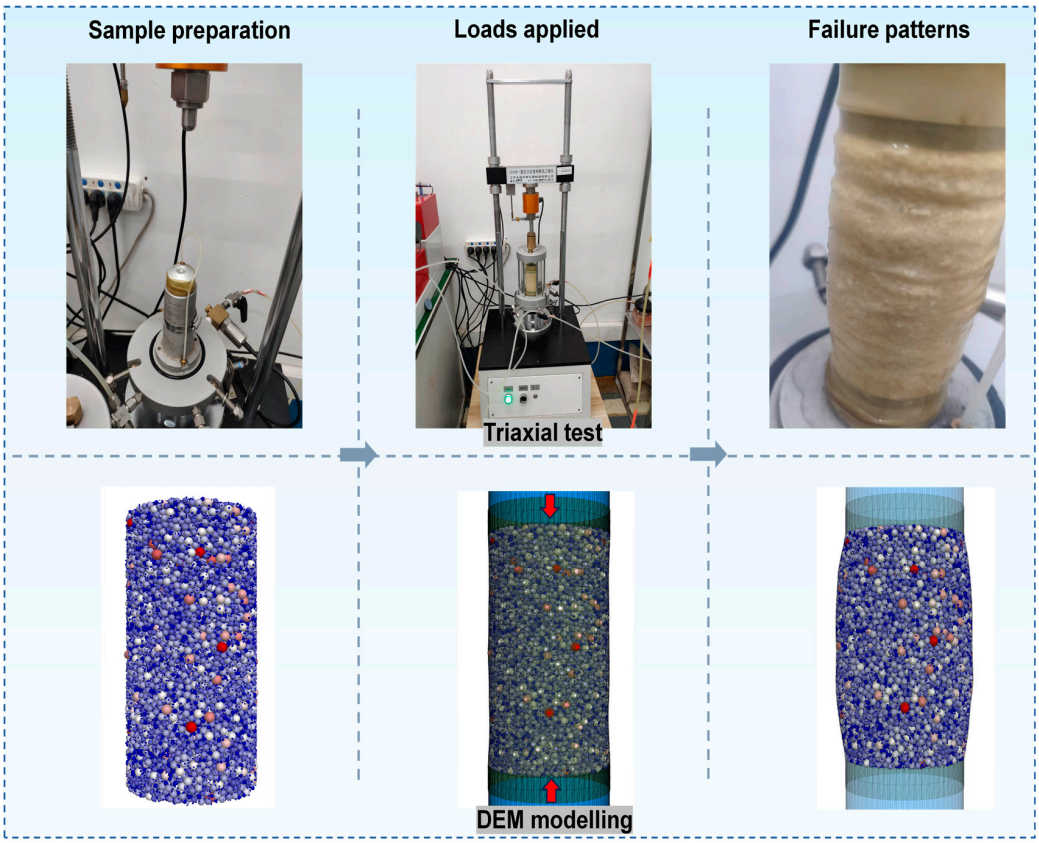

Figure 3. Specimen preparation, load application, and failure modes in triaxial testing and DEM simulation.

2.3. DEM Investigation Arrangements

Further triaxial tests were simulated at high-stress levels, based on the experimental validated DEM model and parameters. As the previous studies [12] presented involved low confining stress (100 kPa~400 kPa), the current study focused on revealing the shear mechanical behavior of unreinforced and reinforced coral sand at high confining pressures (400 kPa~1600 kPa). The specific investigation arrangements are shown in Table 1. Carrying out investigations at high-stress levels made it possible to compare the results with those obtained at lower stress levels, focusing on the influence of the stress level. In addition, the breakage of coral sand particles was significantly more pronounced at high-stress levels, and the distribution pattern of the particle fragments and their influence on the mechanical behavior were also areas of interest.

Table 1. The scheme of the DEM investigation.

Serial Number	Cell Pressures (kPa)	Number of Geogrids	Sources
U1	400	0	Luo et al. [12]
U2	800	0	Current study
U3	1200	0	Current study
U4	1600	0	Current study
R1	400	3	Luo et al. [12]
R2	800	3	Current study
R3	1200	3	Current study
R4	1600	3	Current study

3. Results

3.1. Effect of Confining Pressure on Failure Patterns

The level of confining pressure exerted a significant effect on the failure deformation characteristics of unreinforced and reinforced coral sand specimens. Figure 4 presents the shear deformation and particle displacement of the specimens at 20% axial strain. Three characteristic confining pressures (400 kPa, 800 kPa, and 1600 kPa) were considered to reveal the effect of reinforcement and stress levels on the failure characteristics. In the unreinforced condition (Figure 4a), the failure specimen bulged in the middle, and the particle displacements at the ends were larger. The failure pattern of the specimens remained unchanged as the confining pressure continued to increase, but the particle displacement in the middle of the specimens tended to decrease at high confining pressures. In the three-layer-reinforced condition (Figure 4b), the failure pattern of the specimens differed from that of the unreinforced condition. The particles in the middle of the reinforced specimens were constrained by the geogrid, and the particle displacement was significantly smaller than that of the unreinforced condition. In addition, the tendency of bulging in the middle of the reinforced specimens was reduced relative to the unreinforced condition. At 400 kPa, the deformation in the middle of the reinforced specimens was obviously suppressed, but the bulging deformation at the ends seemed to be more obvious. With the increase in the confining pressure to 1600 kPa, the end deformation of the reinforced specimens was also suppressed, and the bulging deformation of the specimens after failure was relatively low. The failure characteristics presented by the unreinforced and reinforced specimens at different confining pressures indicated that the reinforcement and high confining stresses can significantly inhibit the bulging deformation, especially the significant inhibition of the particle displacement in the central region.

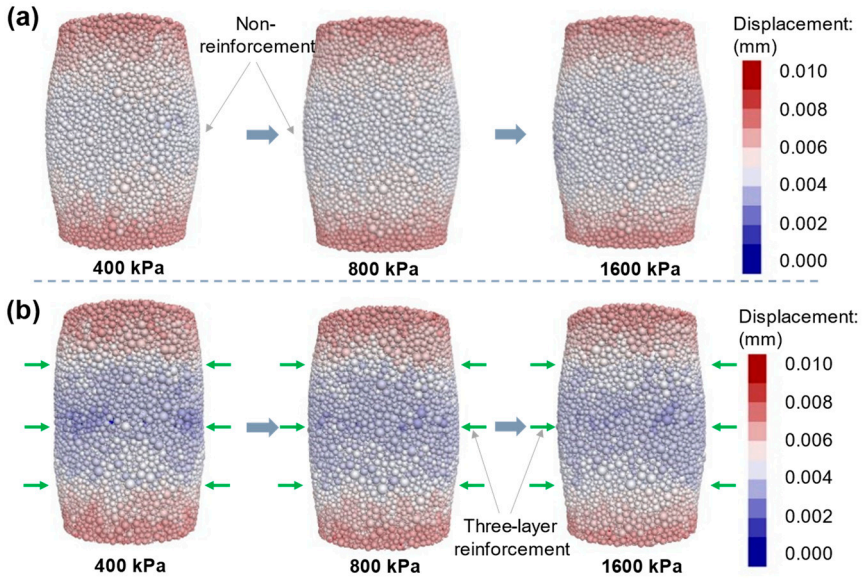

Figure 4. Effect of high confining pressure on failure patterns: (**a**) unreinforced case and (**b**) reinforcement.

3.2. Deviatoric Stress–Axial Strain Responses

The reinforced condition and high confining stresses influenced the failure characteristics of the specimens and further determined their shear mechanical response. The deviatoric stress–axial strain curves for the unreinforced and reinforced conditions are presented in Figure 5. The deviatoric stress–axial strain curves of the unreinforced coral sand showed a peak with the increased confining pressure. Under the 400 kPa confining pressure, the deviatoric stress entered the plateau at 10% axial strain, with no obvious peak. With the increase in the confining pressure to 800 kPa~1600 kPa, the deviatoric stress peaked at 11~12% axial strain, and the softening tendency after the peak increased with the increased confining pressure. For the reinforced specimens, the pattern of the deviatoric

stress–axial strain curve is varied with the increased confining pressure. The deviatoric stress–axial strain curves showed a plateau pattern or a slight hardening trend at 400 kPa to 1600 kPa. In addition, the strength of the reinforced specimens was also higher than that of the unreinforced specimens, but the enhancement was not obvious at high confining pressures. The reinforcement greatly improved the mechanical properties of the specimens while suppressing the bulging deformation, especially the suppression of the softening trend of the deviatoric stress–axial strain curve.

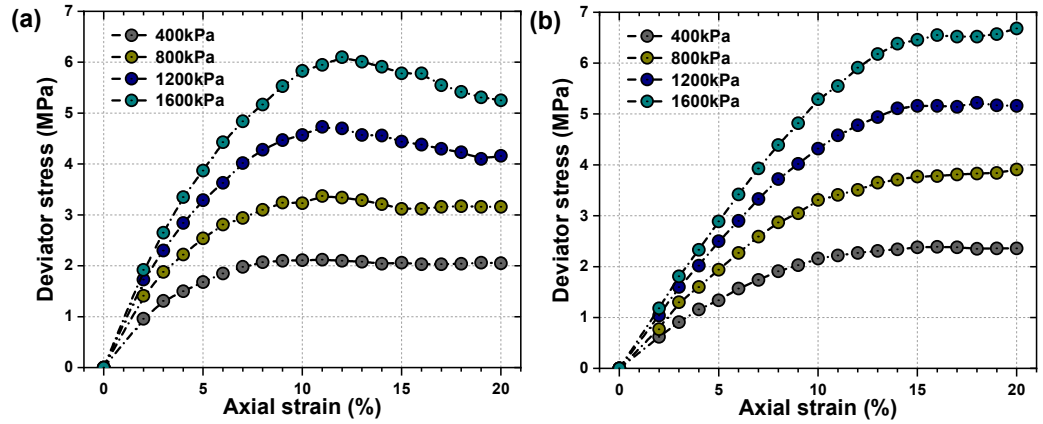

Figure 5. Effect of high confining pressure on deviatoric stress–axial strain curves: (**a**) unreinforced case and (**b**) reinforcement.

3.3. Shear Strength and Parameters

According to the deviatoric stress–axial strain curves, the shear strengths of the unreinforced and reinforced specimens, expressed in terms of large principal stresses, could be obtained. As shown in Figure 6, the difference in shear strength between the reinforced and unreinforced specimens under 400 kPa to 1600 kPa confining pressure was relatively small, and it was maintained at about 500 kPa. Obviously, the high confining pressure stress did not stimulate the reinforcing effect of the geogrid. Under high confining stresses, the occlusion between particles was intensified, and the inter-particle skeleton was the main source of strength. Due to the limited tensile strength of geogrids, even though the geogrid–particle interlocking was enhanced under high stresses, it did not substantially increase the shear strength. Overall, the shear strengths of unreinforced and reinforced specimens under 400 kPa to 1600 kPa confining pressure mainly ranged between around 2 MPa and 8 Mpa.

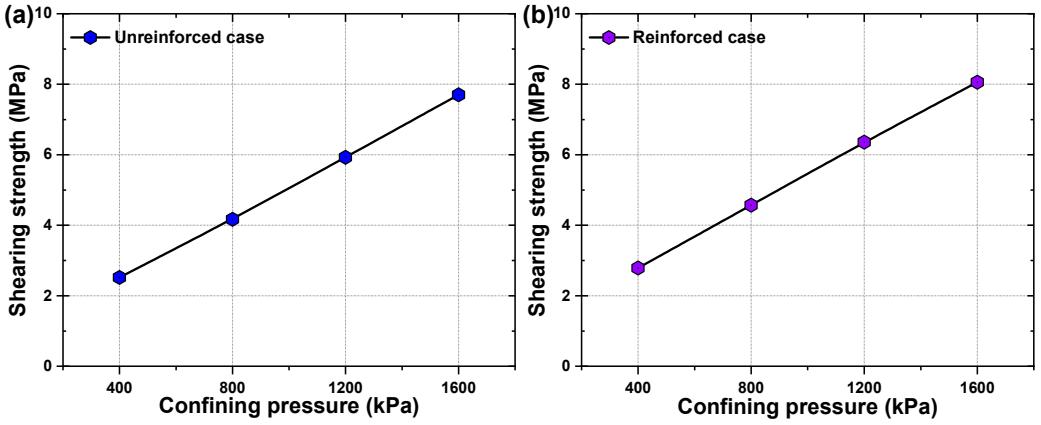

Figure 6. Effect of high confining pressure on the shear strength: (**a**) unreinforced case and (**b**) reinforcement.

Despite the relatively limited shear strength induced by reinforcement at high confining pressure conditions, the effect of reinforcement on the shear mechanical parameters was of interest, especially its difference from that at low confining pressure conditions. For shear strength values in a certain range of confining pressures, they can be expressed by the relationship between the major and minor principal stresses in the limit equilibrium condition:

$$\sigma_1 = \sigma_3 \tan^2(45^\circ + \varphi/2) + 2c_p \tan(45^\circ + \varphi/2) \quad (1)$$

where σ_1 is the large principal stress, which is equal to the sum of the confining pressure and the deviatoric stress, σ_3 is the small principal stress, i.e., equal to the confining pressure, and the parameters c_p and φ are the pseudo-cohesion and the internal friction angle, respectively. The intercept I and slope K were obtained by linear fitting of σ_1 and σ_3 under different confining pressures. Further, the shear mechanical parameters can be calculated based on the following equations [25]:

$$c_p = \frac{I}{2\sqrt{K}} \quad (2)$$

$$\varphi = 2(\arctan\sqrt{K} - 45^\circ) \quad (3)$$

The shear parameters of the reinforced specimens at 400 kPa to 1600 kPa confining pressure were obtained and compared with the results presented by Luo et al. [12] at a low confining pressure (Figure 7). The results showed that the high confining stress affected the internal friction angle of the reinforced coral sand very little, but significantly increased its pseudo-cohesion. Compared with the 100 kPa~400 kPa confining pressure, the internal friction angle only increased by 0.07° at the high confining pressure from 400 kPa to 1600 kPa, which remained almost constant. On the contrary, the pseudo-cohesion under high confining pressure increased by 78.4 kPa compared to that under 100 kPa to 400 kPa confining pressures. It should be noted that the increment of pseudo-cohesion under high confining stress was not entirely the contribution of the geosynthetics, but also related to the enhancement of the occlusion between coral sand particles. At high-stress levels, pseudo-cohesion may be significantly elevated, and this effect was especially pronounced for coral sand particles considering their abundant angularity.

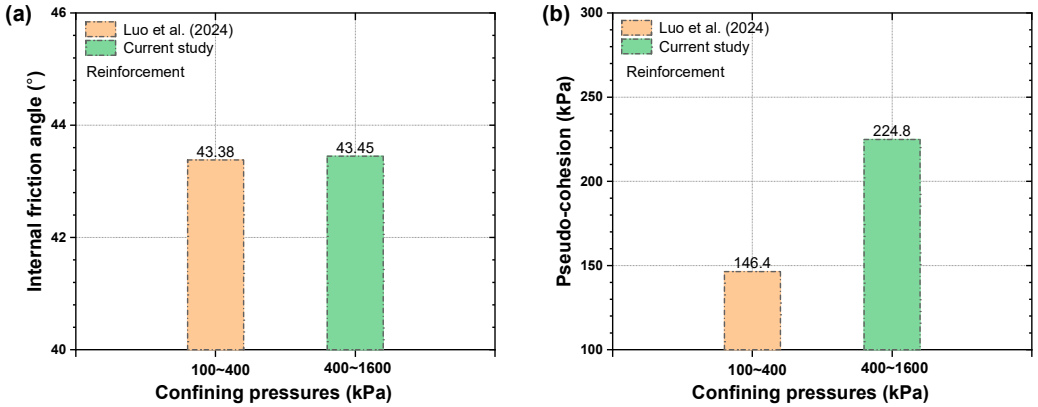

Figure 7. Effect of high confining pressure on the shear mechanical parameters compared with the low pressure condition [12]: (**a**) internal friction angle and (**b**) pseudo-cohesion.

4. Discussion

4.1. Patterns of Inter-Particle Contact Forces

The macroscopic mechanical response is related to the microscopic particle interaction. To further investigate the shear strength mechanism of unreinforced and reinforced specimens under high confining stress, the microscopic contact force chain was analyzed, as shown in Figure 8. The contact force level of the specimens was significantly enhanced with the increase in the confining pressure. At the same confining pressure, the contact force

level of the reinforced specimens was significantly higher than that of the unreinforced specimens. Due to the effect of the geosynthetics, the force chain of the core bearing was distributed in a columnar shape along the central axis of the specimen. On the contrary, the force chains of the unreinforced specimens were distributed more uniformly, including the contact force chains with higher forces. The interlocking effect of the geogrid enhanced the contact stresses of the particles, which in turn led to higher stress levels between the reinforced layers [30]. Since the geogrids can resist the action of the principal stresses, they in turn can mitigate the stress level in the edge region of the specimen. For the unreinforced specimen, the bearing of the specimen was mainly dependent on the inter-granular skeleton, and the stress distribution was more uniform throughout the specimen. Essentially, reinforcement altered the stress distribution pattern of the specimen, and this difference was amplified as the confining stress increased.

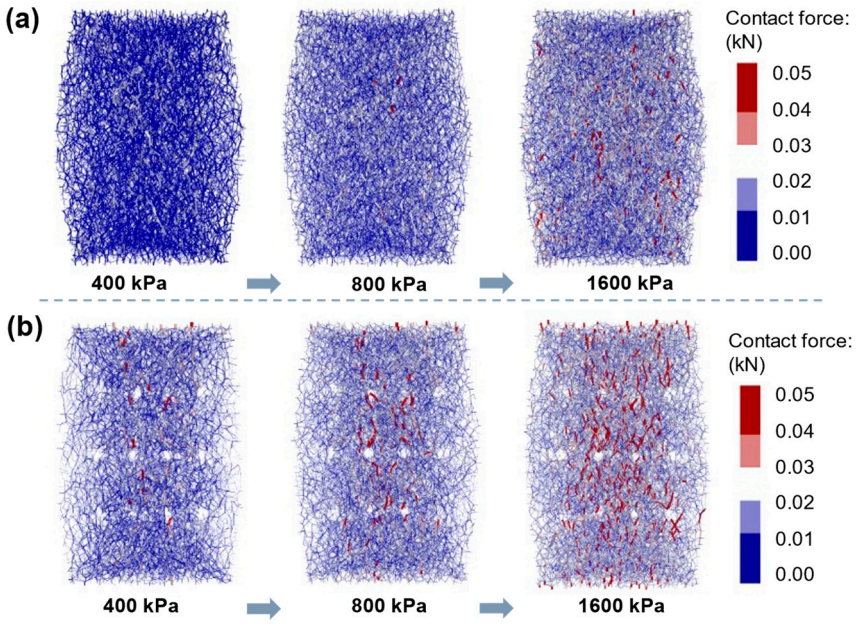

Figure 8. Effect of high confining pressure on microscopic contact force: (**a**) unreinforced case and (**b**) reinforcement.

4.2. Tensile Force Chains of Geogrids

For the reinforced specimens under high confining stress, the distribution patterns of the microscopic contact force and the macroscopic shear mechanical behavior were mainly affected by the geosynthetics. As a reinforced material, the geogrid resisted the large principal stresses during shear by tension resistance. The degree of geogrid tensioning was closely related to the reinforcing effect. Figure 9 presents the microscopic tensile chain of the geogrids under different confining pressures and shear strains. The overall trend was that the tensile force of the geogrids increased with the increasing confining pressure and shear strain. At 6% axial strain (Figure 9a), the effect of a high confining pressure on the tensile force of the geogrid was limited, and the level of tensile force of the geogrid under the confining pressure of 400 kPa~1600 kPa was comparable and mainly lower than 0.1 kN. When the axial strain was increased to 14% (Figure 9b), the tensile force of the geogrid showed a slight increasing trend with the increase in the confining pressure. Meanwhile, the tensile force at most locations of the geogrid reached 0.1 kN under 400 kPa~1600 kPa confining pressure, and the tensile effect of the geogrid began to play a reinforcing role. At the end of shear (Figure 9c), the tensile force of the geogrids increased significantly with the increase in the confining pressure, especially as the tensile force of the geogrids reached more than 0.2 kN at 1600 kPa. In addition, the tensile force of different geogrid layers under this shear strain was not consistent, showing that the middle layer was more obviously

subjected to tension, especially for the high confining pressure condition (e.g., 1600 kPa). The contribution of reinforcement to shear strength and deformation can be indirectly characterized by the tensile force of the geogrid. Higher geogrid tension resistance provided stronger resistance to large principal stresses and bulging deformations, and thus the effect of reinforcement was more prominent. Nevertheless, the contribution of reinforcement to shear strength was relatively low for high-stress conditions, thus presenting the strength law shown in Figure 6. For high-stress conditions, increasing the tensile strength of the geosynthetics may be the way to substantially increase the shear strength and resistance to deformation of the reinforced coral sand.

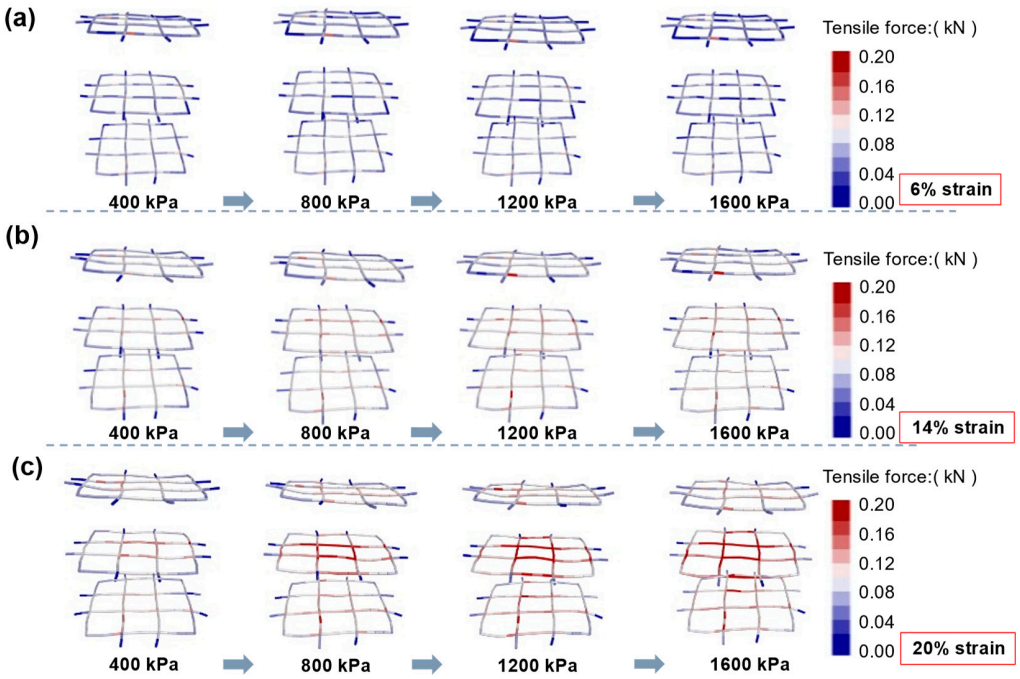

Figure 9. Tensile force of geogrids under varied confining pressures and shear strains: (**a**) 6% strain, (**b**) 14% strain, and (**c**) 20% strain.

4.3. Evolution of Particle Fragments

Particle breakage is a fundamental property of coral sand, and it has a certain impact on stress and deformation behavior [4,9]. During the shearing process, particles underwent a certain amount of particle breakage with the increasing shear strain and stress. Particle breakage under high stress was of concern. Figure 10 shows the particle fragment distributions of unreinforced and reinforced coral sands under different shear strains at a high confining pressure of 1600 kPa. Under both unreinforced and reinforced conditions, the particle fragments were mainly concentrated in the middle of the sample, with fewer distributed at the ends. For axial strains less than 10%, the number of particle fragments was relatively limited. After the axial strain exceeded 10%, the number of particle fragments increased sharply. Overall, the number of particle fragments in the unreinforced specimen under high stress was slightly higher than that in the reinforced specimen, which is different from the rule under a low confining pressure. Under a confining pressure of 1600 kPa, the degree of particle breakage was high and mostly concentrated in the middle area of the sample. However, the three-layer geogrid occupied a certain volume, resulting in a decrease in the number of particles in the middle area of the sample. In addition, the geogrid was relatively soft and highly ductile, and the number of crushed particles near the geogrid layer was even lower. This difference means that the number of particle fragments in the reinforced sample under high-stress conditions was slightly lower than that in the unreinforced sample.

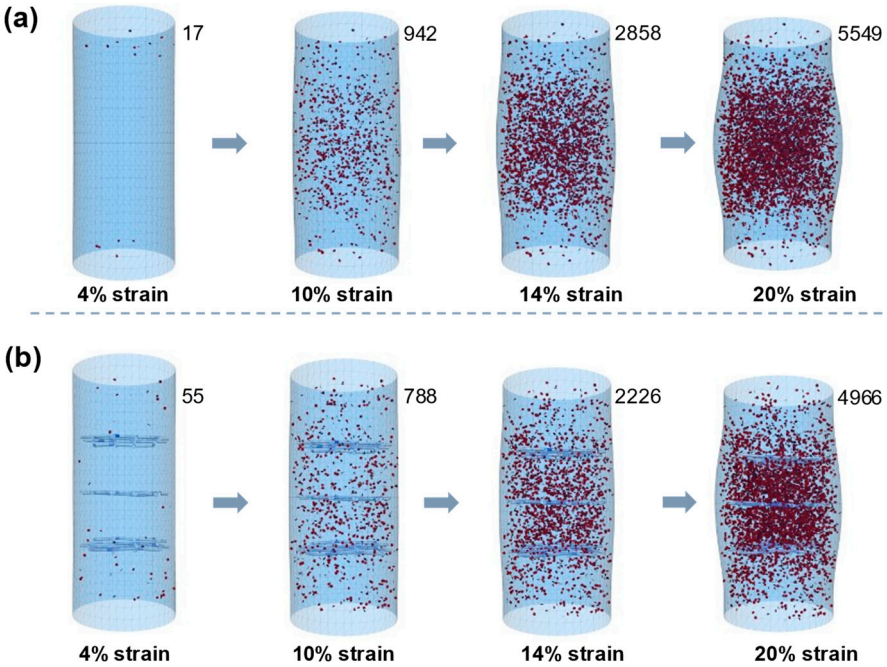

Figure 10. 3D distribution of particle fragments under 1600 kPa confining pressure and different axial strains: (**a**) unreinforced case and (**b**) reinforcement.

In addition to shear strain, the confining pressure also largely influenced the final particle fragment distribution of the unreinforced and reinforced samples (Figure 11). At confining pressures of 400 kPa and 800 kPa, the number of particle fragments in the reinforced specimen was slightly greater than in the unreinforced specimen. As the confining pressure reached 1200 kPa, the number of particle fragments in the unreinforced specimen prevailed. As the confining pressure continued to increase, the rate of increase in particle fragments began to decrease, especially in the reinforced specimen. The particle fragments under a high confining pressure were more concentrated in the middle area of the sample, while under a 400 kPa confining pressure, the particle fragments were relatively evenly distributed. Compared with the sample under a 400 kPa confining pressure, the increase in particle fragments under a high confining pressure mainly occurred in the central region of the sample, which was related to the larger shear stress in this region. For example, the contact force distribution pattern in Figure 8 shows that the contact force in the central region of the sample under a high confining pressure was large. In addition, the bulging in the central region of the sample will also lead to an increase in relative shear displacement between particles in this region, which in turn makes particle breakage more likely to occur.

4.4. Gradation Curve After Crushing

Particle breakage led to changes in the initial grading curve, which in turn affected the macroscopic mechanical behavior. To further reveal the characteristics of coral sand particles under a high confining pressure, the particle size distribution of some representative samples under different shear strains was statistically analyzed, and the results are shown in Figure 12. Under confining pressures of 800 kPa and 1600 kPa, the PSD curves of the unreinforced and reinforced samples were similar in pattern, and the degree of breakage was comparable. Particle breakage increased with the increasing shear strain and confining pressure, as indicated by the shift in the PSD curve. The core breakage zone occurred in the 0.5 mm to 1 mm range, which was related to the initial angular structure of the particles. The initial particle corner diameter was 1/4 of the host particle diameter, i.e., the maximum diameter of the corner was less than 1 mm. Therefore, the gradation interval below 1 mm changed greatly when particle breakage occurred. It should be noted that the actual distribution of coral sand particles and corners was more complex, and the PSD after breakage may differ from the pattern in Figure 12.

Nevertheless, Figure 12 shows the evolution of the gradation of unreinforced and reinforced coral sand with axial strain under a high confining pressure, which is of great importance for understanding the breakage behavior under a high confining pressure.

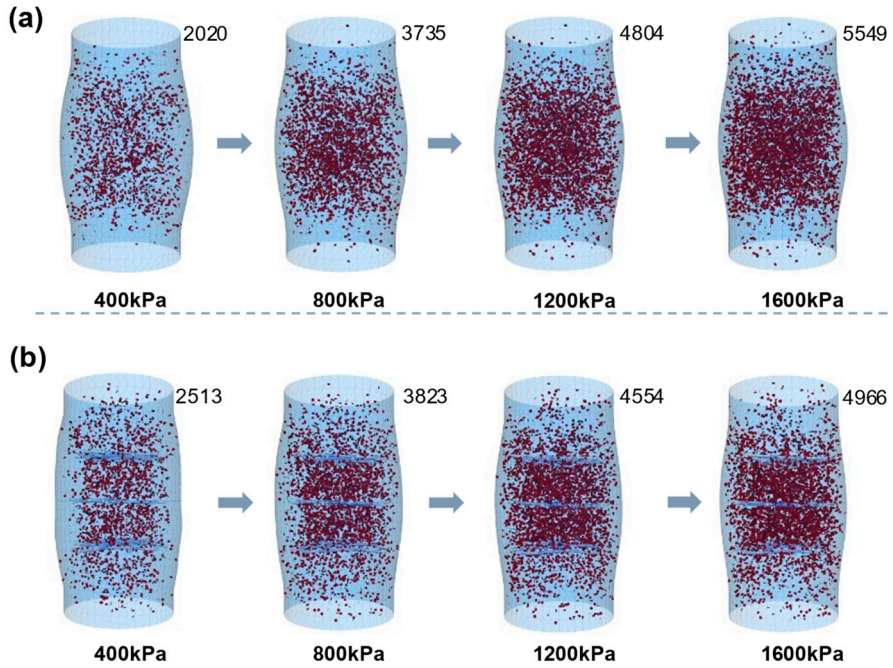

Figure 11. 3D distribution of particle fragments under 20% shear strain and different confining pressures: (**a**) unreinforced case and (**b**) reinforcement.

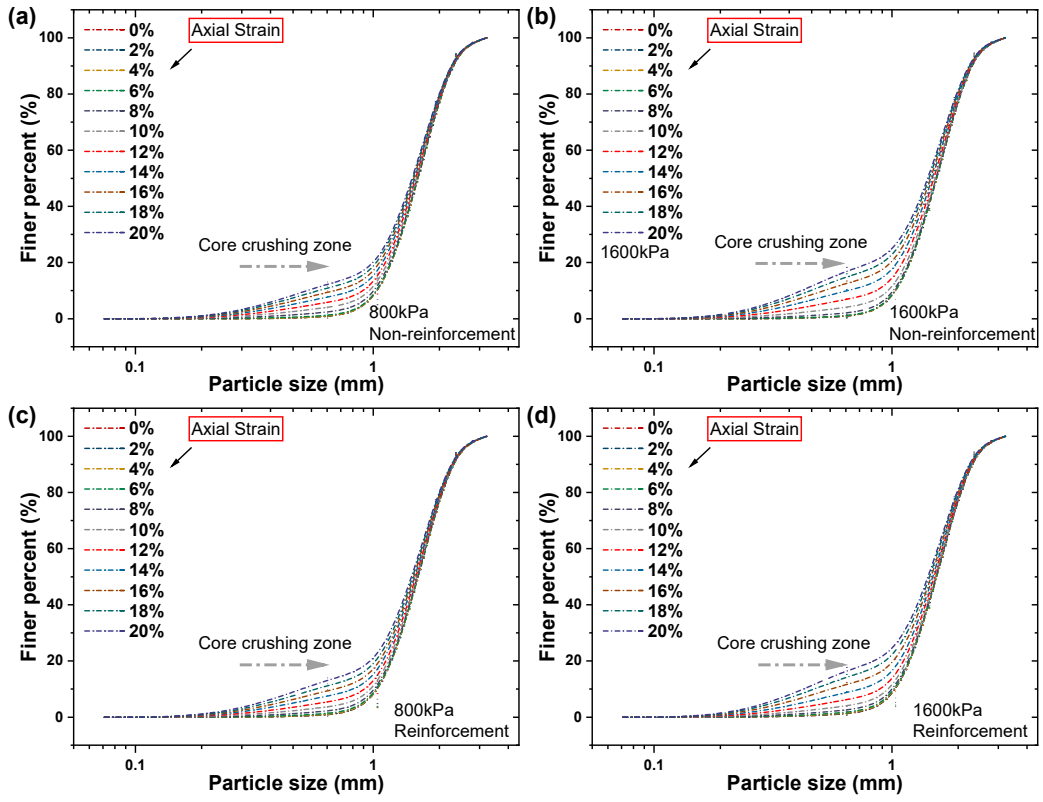

Figure 12. Effects of high confining pressure and reinforcement on the particle size distribution: (**a**) unreinforced case, **c** = 800 kPa, (**b**) unreinforced case, **c** = 1600 kPa, (**c**) reinforced case, **c** = 800 kPa, and (**d**) reinforced case, **c** = 1600 kPa.

4.5. Relative Breakage Index

The PSD curve can be used to quantitatively characterize the degree of particle size reduction. Hardin [40] proposed the relative breakage index B_r to characterize the degree of breakage, which is defined as follows:

$$B_r = \frac{B_t}{B_p} \tag{4}$$

where B_t is the total breakage and B_p is the breakage potential corresponding to the initial grading curve. For the grading curve shown in Figure 12, the relative breakage index corresponding to each PSD curve can be calculated using the method provided by Hardin [40], and the results are shown in Figure 13. Overall, the relative breakage index increased with the increase in axial strain; especially, after the shear strain exceeded 10%, the growth rate was more prominent. For both the unreinforced and reinforced specimens, the increase in B_r under a confining pressure of 1600 kPa was relatively limited. Among them, the increase in B_r of the reinforced specimen was relatively small after exceeding a 1200 kPa confining pressure, indicating that the effect of a high confining pressure on B_r was limited. In addition, Figure 13 also shows the final relative breakage index when 20% shear strain was reached. Under confining pressures of 400 kPa to 1200 kPa, the final B_r of the reinforced specimen was slightly higher than that of the unreinforced specimen. In contrast, the B_r of the unreinforced specimen under a confining pressure of 1600 kPa was more prominent, reaching about 8%. This is further evidence that particle breakage in the reinforced specimen may be relatively smaller under a high confining pressure. At relatively low confining pressures, the reinforcing effect increased the shear stress, and thus the degree of particle breakage. However, when the confining pressure was high enough, the breakage potential of the particles due to the geogrid volume decreased, and the geogrid also limited the shearing and misalignment of the particles. These effects caused the final particle breakage of the reinforced sample to be slightly lower than that of the unreinforced condition. Therefore, understanding the effect of high confining pressures on the breakage behavior of unreinforced and reinforced coral sand is of great significance for future reinforcement design and understanding of the mechanical mechanism.

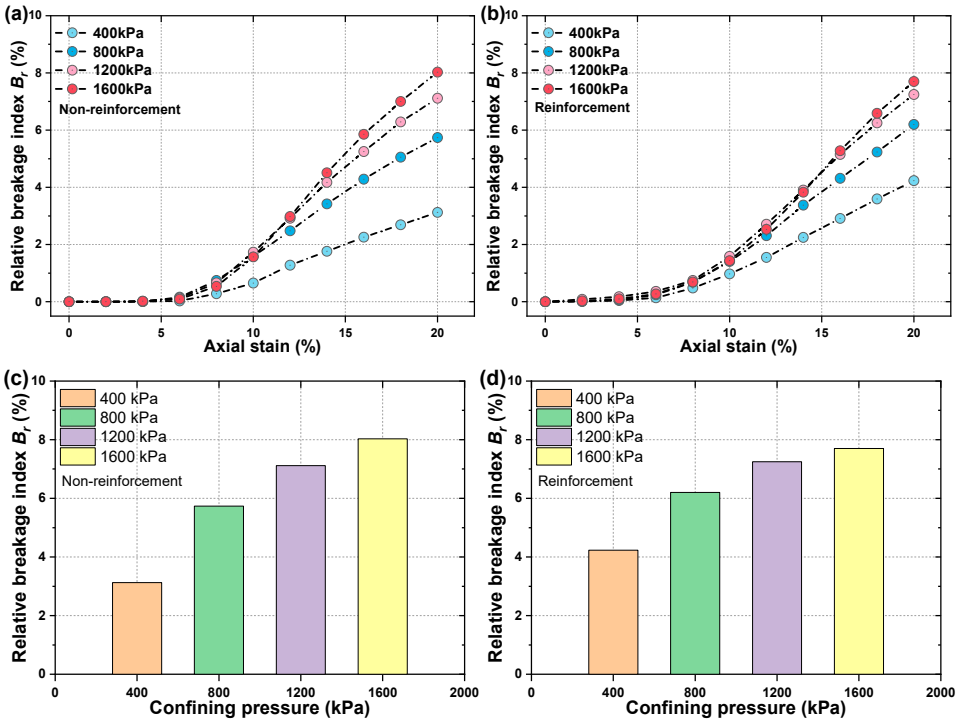

Figure 13. Evolution of the relative breakage index B_r: (**a**,**b**) evolution of the relative breakage index with axial strain in unreinforced and reinforced cases, and (**c**,**d**) final value of the relative breakage index in unreinforced and reinforced cases.

This study compared the macroscopic shear mechanical behavior, microscopic stress characteristics, and particle breakage of unreinforced and reinforced coral sand in a high confining stress interval using a three-dimensional DEM simulation. These efforts further enhanced the understanding of the shear behavior of unreinforced and reinforced coral sands, which is important for future island and coastal engineering construction. Nevertheless, the influence mechanism of particle breakage on the macro- and micro-behaviors still needs to be further explored under high-stress conditions to enhance the understanding and optimal design of the bearing and deformation behaviors of geo-structures related to unreinforced and reinforced coral sands.

5. Conclusions

This work investigated the macro/micro-shear mechanical behavior of unreinforced and geosynthetic-reinforced coral sands under the influence of high confining stresses using 3D DEM simulations that were validated by laboratory triaxial tests. The main insights obtained from these works were as follows:

(1) The high confining stress and reinforcement could inhibit the bulging deformation of the triaxial specimens, especially by reducing the particle displacement in the central region of the specimens. In the unreinforced condition, the deviatoric stress–axial strain curves presented obvious peaks at high confining pressures, and the softening tendency was obvious. On the contrary, the deviatoric stress–axial strain curve in the reinforced condition was without peaks and showed a slight hardening or plateau pattern. Overall, the shear strength in the reinforced condition was slightly greater than that in the unreinforced condition, but the contribution of the reinforcement to the shear strength was still limited under the high confining pressure. The internal friction angle in the high confining pressure condition was close to that in the low confining pressure condition, but the pseudo-adhesion in the high confining pressure condition showed a certain increasing trend, which originated from the combined effect of reinforcement and inter-particle occlusion enhancement.

(2) High confining stresses and reinforcement affected the micromechanical characteristics of coral sand and geogrids, as evidenced by changes in contact force patterns and stress levels. The force chains with greater forces in the reinforced specimens under high confining pressure were dominantly distributed in a columnar pattern along the specimen's central axis, whereas the force chains in the unreinforced specimens were uniformly distributed along the entire specimen. The effect of the confining pressure on the geogrid tension was relatively insignificant at low shear strain. With the increase in shear strain in this triaxial test, the tensile force of the geogrid under a high confining pressure increased significantly, and the tensile resistance of the middle layer was relatively greater. Therefore, the geogrid layer played more of a role in the shear strength and deformation suppression under high confining stress.

(3) The distribution of particle fragments under high confining stress was related to the shear strain and the reinforcement condition. With the increase in the confining pressure, the number of particle fragments in the unreinforced specimens instead dominated. The PSD curves at each shear strain indicated that the particle size interval in which particle breakage occurred was mainly from 0.5 mm to 1 mm. The level of confining pressure strongly influenced the PSD curves, whereas the effect of reinforcement on the PSD curves was very limited at the same confining pressure. The statistically based relative breakage index indicated that the final B_r of the reinforced specimens at a 1200 kPa confining pressure was slightly larger, while it was slightly smaller than that of the unreinforced specimens at 1600 kPa. These results demonstrated that the effect of reinforcement on the degree of particle breakage was dependent on the level of the confining pressure.

Author Contributions: Methodology, Z.C.; Investigation, L.L., Z.C., X.D. and Q.O.; Writing—original draft, L.L.; Writing—review & editing, L.L., Z.C., X.D. and Q.O.; Funding acquisition, Z.C. All authors have read and agreed to the published version of the manuscript.

Funding: This work was supported by the State Key Laboratory of Precision Blasting and the Hubei Key Laboratory of Blasting Engineering, Jianghan University (No. PBSKL2022B02), and the National Natural Science Foundation of China (No. 52278331).

Institutional Review Board Statement: Not applicable.

Informed Consent Statement: Not applicable.

Data Availability Statement: Data are contained within the article.

Conflicts of Interest: The authors declare that they have no known competing financial interests or personal relationships that could have appeared to influence the work reported in this paper.

References

1. Wu, Q.; Ding, X.M.; Zhang, Y.L.; Chen, Z.X. Comparative Study on Seismic Response of Pile Group Foundation in Coral Sand and Fujian Sand. *J. Mar. Sci. Eng.* **2020**, *8*, 189. [CrossRef]
2. Wang, X.-Z.; Jiao, Y.-Y.; Wang, R.; Hu, M.-J.; Meng, Q.-S.; Tan, F.-Y. Engineering characteristics of the calcareous sand in Nansha Islands, South China Sea. *Eng. Geol.* **2011**, *120*, 40–47. [CrossRef]
3. Wang, X.; Wu, Y.; Cui, J.; Zhu, C.Q.; Wang, X.Z. Shape Characteristics of Coral Sand from the South China Sea. *J. Mar. Sci. Eng.* **2020**, *8*, 803. [CrossRef]
4. Shahnazari, H.; Rezvani, R. Effective parameters for the particle breakage of calcareous sands: An experimental study. *Eng. Geol.* **2013**, *159*, 98–105. [CrossRef]
5. Lv, Y.; Liu, J.; Xiong, Z. One-dimensional dynamic compressive behavior of dry calcareous sand at high strain rates. *J. Rock Mech. Geotech. Eng.* **2019**, *11*, 192–201. [CrossRef]
6. Coop, M.R.; Sorensen, K.K.; Freitas, T.B.; Georgoutsos, G. Particle breakage during shearing of a carbonate sand. *Geotechnique* **2004**, *54*, 157–163. [CrossRef]
7. Shahnazari, H.; Rezvani, R.; Tutunchian, M.A. Post-cyclic volumetric strain of calcareous sand using hollow cylindrical torsional shear tests. *Soil Dyn. Earthq. Eng.* **2019**, *124*, 162–171. [CrossRef]
8. Tian, Y.H.; Cassidy, M.J. Pipe-Soil Interaction Model Incorporating Large Lateral Displacements in Calcareous Sand. *J. Geotech. Geoenviron. Eng.* **2011**, *137*, 279–287. [CrossRef]
9. OuYang, H.R.; Dai, G.L.; Qin, W.; Zhang, C.F.; Zhu, W.B.; Gong, W.M. Experimental study on the mechanical behaviors and particle breakage characteristics of calcareous sand from South China Sea under repeated one-dimensional impacts. *Acta Geotech.* **2022**, *17*, 3927–3946. [CrossRef]
10. He, S.H.; Goudarzy, M.; Ding, Z.; Sun, Y.F. Strength, Deformation, and Particle Breakage Behavior of Calcareous Sand: Role of Anisotropic Consolidation. *J. Geotech. Geoenviron. Eng.* **2023**, *149*, 04023002. [CrossRef]
11. Xiao, Y.; Sun, Y.; Zhou, W.; Shi, J.Q.; Desai, C.S. Evolution of Particle Shape Produced by Sand Breakage. *Int. J. Geomech.* **2022**, *22*, 04022003. [CrossRef]
12. Luo, Z.G.; Ding, X.M.; Ou, Q.; Lu, Y.W. Macro-microscopic mechanical behavior of geogrid reinforced calcareous sand subjected to triaxial loads: Effects of aperture size and tensile resistance. *Geotext. Geomembr.* **2024**, *52*, 526–541. [CrossRef]
13. Peng, Y.; Ding, X.M.; Yin, Z.Y.; Wang, P. Micromechanical analysis of the particle corner breakage effect on pile penetration resistance and formation of breakage zones in coral sand. *Ocean Eng.* **2022**, *259*, 111859. [CrossRef]
14. Shi, D.D.; Cao, D.; Deng, Y.B.; Xue, J.F. DEM investigations of the effects of intermediate principal stress ratio and particle breakage on the critical state behaviors of granular soils. *Powder Technol.* **2021**, *379*, 547–559. [CrossRef]
15. Gao, R.; Ye, J.H. Mechanical behaviors of coral sand and relationship between particle breakage and plastic work. *Eng. Geol.* **2023**, *316*, 107063. [CrossRef]
16. Lin, L.; Li, S.; Huo, L.Y.; Liu, X. Study on the relationship between fractal dimension and particle fragmentation for marine coral sand under impact load. *Ocean Eng.* **2023**, *286*, 115442. [CrossRef]
17. Liu, L.; Liu, H.L.; Stuedlein, A.W.; Evans, T.M.; Xiao, Y. Strength, stiffness, and microstructure characteristics of biocemented calcareous sand. *Can. Geotech. J.* **2019**, *56*, 1502–1513. [CrossRef]
18. Peng, Y.; Yin, Z.Y.; Ding, X.M. Micromechanical analysis of the particle corner breakage effect on pile load performance in coral sand. *Acta Geotech.* **2023**, *18*, 6353–6370. [CrossRef]
19. Gu, J.X.; Zeng, C.; Lyu, H.B.; Yang, J.Y. Effects of cement content and curing period on strength enhancement of cemented calcareous sand. *Mar. Georesources Geotechnol.* **2021**, *39*, 1083–1095. [CrossRef]
20. Tavakol, K.; Bayat, M.; Nadi, B.; Ajalloeian, R. Combined Influences of Cement, Rice Husk Ash and Fibre on the Mechanical Characteristics of a Calcareous Sand. *Ksce J. Civ. Eng.* **2023**, *27*, 3729–3739. [CrossRef]
21. Kou, H.L.; Li, Z.D.; Liu, J.H.; An, Z.T. Effect of MICP-recycled shredded coconut coir (RSC) reinforcement on the mechanical behavior of calcareous sand for coastal engineering. *Appl. Ocean Res.* **2023**, *135*, 103564. [CrossRef]

22. Xiao, Y.; Zhang, Z.C.; Stuedlein, A.W.; Evans, T.M. Liquefaction Modeling for Biocemented Calcareous Sand. *J. Geotech. Geoenviron. Eng.* **2021**, *147*, 04021149. [CrossRef]
23. Rezvani, R. Shearing response of geotextile-reinforced calcareous soils using monotonic triaxial tests. *Mar. Georesources Geotechnol.* **2019**, *38*, 238–249. [CrossRef]
24. Zhou, L.; Chen, J.F.; Wang, R. Influence of geosynthetics reinforcement on liquefaction and post-liquefaction behaviors of calcareous sand. *Ocean Eng.* **2024**, *293*, 116598. [CrossRef]
25. Luo, Z.G.; Ding, X.M.; Ou, Q.; Jiang, C.Y.; Fang, H.Q. Experimental study on strength and deformation characteristics of coral sand reinforced by geogrid. *Rock Soil Mech.* **2023**, *44*, 1053–1064. [CrossRef]
26. Zeng, H.; Yin, L.-Y.; Tang, C.-S.; Zhu, C.; Cheng, Q.; Li, H.; Lv, C.; Shi, B. Tensile behavior of bio-cemented, fiber-reinforced calcareous sand from coastal zone. *Eng. Geol.* **2021**, *294*, 106390. [CrossRef]
27. Akosah, S.; Zhou, L.; Chen, J.F.; Lawer, A.K. Experimental investigation on cyclic behavior of geogrid-reinforced coral sand from the South China Sea. *Mar. Georesources Geotechnol.* **2024**, *42*, 707–720. [CrossRef]
28. Goodarzi, S.; Shahnazari, H. Strength enhancement of geotextile-reinforced carbonate sand. *Geotext. Geomembr.* **2019**, *47*, 128–139. [CrossRef]
29. Lei, X.; Lin, S.; Meng, Q.; Liao, X.; Xu, J. Influence of different fiber types on properties of biocemented calcareous sand. *Arabian J. Geosci.* **2020**, *13*, 317. [CrossRef]
30. Ding, X.M.; Luo, Z.G.; Ou, Q. Mechanical property and deformation behavior of geogrid reinforced calcareous sand. *Geotext. Geomembr.* **2022**, *50*, 618–631. [CrossRef]
31. Luo, Z.G.; Ding, X.M.; Ou, Q.; Fang, H.Q. Bearing capacity and deformation behavior of rigid strip footings on coral sand slopes. *Ocean Eng.* **2023**, *267*, 113317. [CrossRef]
32. Zhou, L.; Chen, J.F.; Zhuang, X.Y. Undrained cyclic behaviors of fiber-reinforced calcareous sand under multidirectional simple shear stress path. *Acta Geotech.* **2023**, *18*, 2929–2943. [CrossRef]
33. Hu, F.H.; Fang, X.W.; Yao, Z.H.; Wu, H.R.; Shen, C.N.; Zhang, Y.T. Experiment and discrete element modeling of particle breakage in coral sand under triaxial compression conditions. *Mar. Georesources Geotechnol.* **2021**, *41*, 142–151. [CrossRef]
34. Ou, Q.; Li, Y.F.; Yang, Y.; Luo, Z.G.; Han, S.K.; Zou, T. Mechanical Property of Biomodified Geogrid and Reinforced Calcareous Sand. *Geofluids* **2022**, *2022*, 3768967. [CrossRef]
35. Zeng, K.F.; Liu, H.B. Effect of Inherent Anisotropy on the Triaxial Compression Behavior of Coral Sand. *Int. J. Geomech.* **2023**, *23*, 04023033. [CrossRef]
36. Xu, L.J.; Wang, R.; Liu, Q.B.; Chen, J.F.; Wang, X.Z.; Meng, Q.S. Effect of particle size distribution on monotonic direct shear characteristics of geotextile/geogrid-calcareous sand interface. *Appl. Ocean Res.* **2023**, *137*, 103601. [CrossRef]
37. Luo, Z.G.; Ding, X.M.; Zhang, X.H.; Ou, Q.; Yang, F.C.; Zhang, T.; Cao, G.W. Experimental and numerical investigation of the bearing capacity and deformation behavior of coral sand foundations under shallow footing loads. *Ocean Eng.* **2024**, *310*, 118601. [CrossRef]
38. Potyondy, D.O.; Cundall, P.A. A bonded-particle model for rock. *Int. J. Rock Mech. Min. Sci.* **2004**, *41*, 1329–1364. [CrossRef]
39. Wang, Z.J.; Jacobs, F.; Ziegler, M. Visualization of load transfer behaviour between geogrid and sand using PFC2D. *Geotext. Geomembr.* **2014**, *42*, 83–90. [CrossRef]
40. Hardin, B.O. Crushing of Soil Particles. *J. Geotech. Eng.* **1985**, *111*, 1177–1192. [CrossRef]